HAL open science

Magnetic damping of ferromagnetic and exchange resonance modes in a ferrimagnetic insulator

Marwan Deb, Pierre Molho, Bernard Barbara

To cite this version:

Marwan Deb, Pierre Molho, Bernard Barbara. Magnetic damping of ferromagnetic and exchange resonance modes in a ferrimagnetic insulator. Physical Review B, 2022, 105 (1), pp.014432. 10.1103/physrevb.105.014432 . hal-04317079

HAL Id: hal-04317079

https://hal.science/hal-04317079v1

Submitted on 1 Dec 2023

HAL is a multi-disciplinary open access archive for the deposit and dissemination of scientific research documents, whether they are published or not. The documents may come from teaching and research institutions in France or abroad, or from public or private research centers.

L'archive ouverte pluridisciplinaire **HAL**, est destinée au dépôt et à la diffusion de documents scientifiques de niveau recherche, publiés ou non, émanant des établissements d'enseignement et de recherche français ou étrangers, des laboratoires publics ou privés.

Magnetic damping of ferromagnetic and exchange resonance modes in a ferrimagnetic insulator

Marwan Deb,[1,2,*] Pierre Molho,[3,4] and Bernard Barbara[3,4]

[1]*Institut für Physik und Astronomie, Universität Potsdam, Karl-Liebknecht-Straße 24-25, 14476 Potsdam, Germany*
[2]*Unité Mixte de Physique, CNRS, Thales, Université Paris-Saclay, 91767 Palaiseau, France*
[3]*CNRS, Institut Néel, F-38042 Grenoble, France*
[4]*Université Grenoble Alpes, Institut Néel, F-38042 Grenoble, France*

(Received 5 October 2021; revised 15 December 2021; accepted 15 January 2022; published 26 January 2022)

Understanding the damping is an important fundamental problem with widespread implications in magnetic technology. Ferrimagnetic materials offer a rich platform to explore not only the damping of the ferromagnetic mode, but also the damping of the high-frequency exchange mode very promising for ultrafast devices. Here we use time-resolved magneto-optical Kerr effect to investigate the ferromagnetic and exchange resonance modes and their damping in the bismuth-doped gadolinium iron garnet over a broad range of magnetic fields (0–10 T) and temperatures (50–300 K) including the magnetization and angular compensation points. These two resonance modes are excited via the inverse Faraday effect and unambiguously identified by their distinct frequency dependence on temperature and magnetic field. The temperature-dependent measurements in the external magnetic field $H_{\mathrm{ext}} = 2\,\mathrm{T}$ revealed that the intrinsic damping of the ferromagnetic mode is always smaller than the one of the exchange modes and both have a maximum near the angular compensation point. These results are fully consistent with recent predictions of atomistic simulations and a theory based on two-sublattice Landau-Lifshitz-Bloch equation. We also demonstrate that the damping of these modes varies differently as a function of H_{ext}. We explain the observed behaviors by considering the different features of the effective fields defining the precession frequencies of the ferromagnetic and exchange modes.

DOI: 10.1103/PhysRevB.105.014432

I. INTRODUCTION

Due to its crucial role in magnetization dynamics, magnetic damping has attracted a great deal of attention since its introduction by Gilbert and Bloch in the middle of the 19th century [1,2]. Indeed, magnetic damping is one of the crucial parameters defining the energy efficient and operation speed in most past and present magnetic technologies, including those based on domain-wall motion [3–5], magnetization switching [6,7], and spin-wave propagation [8,9]. To satisfy the increasing demand for more energy-efficient and faster technologies, studying, understanding, and controlling the magnetic damping are nowadays subjects of great interest in almost all major fields of modern magnetism such as spintronics [10–14], magnonics [8,9,15,16], and ultrafast magnetism [17–21]. For instance, in magnonics, a low magnetic damping is desired to realize energy-efficient spin waves-based data transport and processing technologies [8,16,22,23]. On the other hand, a high damping is essential to obtain an ultrafast ringing-free precessional switching [6], which is very important for faster data storage and spintronic memory devices.

Recently, there has been a huge renewed interest in rare-earth (RE)–transition-metal (TM) ferrimagnets, due to the discovery of many unique and interesting magnetization dynamic phenomena at the magnetization compensation temperature T_{M} (where $M_{\mathrm{RE}} = M_{\mathrm{TM}}$) and/or at the angular momentum compensation temperature T_{A} (where $M_{\mathrm{RE}}/\gamma_{\mathrm{RE}} = M_{\mathrm{TM}}/\gamma_{\mathrm{TM}}$, γ_{RE}, and γ_{TM} being the gyromagnetic ratios). In particular, the possibility to reverse the magnetization of RE-TM metallic alloys near T_{M} using femtosecond laser or hot-electron pluses without requiring any external magnetic field [24,25] was demonstrated. Femtosecond laser pulse has also been used to trigger a magnetization reversal across T_{M} of RE-TM ferrimagnetic insulating [26] and metallic [27] films. Beside the magnetization reversal dynamics, interesting experiments have shown that domain-wall mobility reaches a maximum at T_{A} [28,29]. Moreover, an enhancement of the spin-transfer torque and spin-orbit torque has been reported in the vicinity of T_{M} and T_{A} [30–32]. These important phenomena make RE-TM ferrimagnets a promising candidate for future ultrafast data storage and spintronics technologies.

Despite the important criterion related to T_{M} and/or T_{A} in all the above-mentioned phenomena, exploring the magnetic damping near these temperatures has been limited to only few studies [17,18,33], which show some disagreements between the experimental results themselves as well as between the experimental results and the theoretical predictions. Indeed, the time-resolved magneto-optical experiments in GdFeCo by Stanciu *et al.* [17] and in CoGd by Binder *et al.* [18] show a finite maximum of the damping related to the ferromagnetic resonance mode at T_A, which is in disagreement with the earlier theoretical prediction of a divergence used to discuss the data [see Eq. (5)]. More surprisingly, in 2019, Kim *et al.* [33] extracted from the field-driven domain-wall motion in GdFeCo a constant ferromagnetic damping over T_{A}. Even more important, these studies have been limited to the damping of the ferromagnetic mode in metallic ferrimagnets [17,18,33] and did not explore the damping of the exchange

*madeb@uni-potsdam.de

 ©2022 American Physical Society

mode. Therefore, extending the investigations to the damping of both ferromagnetic and exchange modes as well as to other RE-TM ferrimagnetic systems like the insulating oxide of gadolinium iron garnet is important to improve our fundamental understanding of ultrafast magnetization dynamics in ferrimagnets.

In this paper, we carefully investigate the ferromagnetic and exchange resonance modes and their damping in the RE-TM ferrimagnetic insulator of a Bi-dopped gadolinium iron garnet using the time-resolved magneto-optical Kerr effect. We show that femtosecond laser pulses trigger both ferromagnetic and exchange resonance modes over a broad range of magnetic fields (0–10 T) and temperatures (50–300 K) including T_M and T_A. We identify the ferromagnetic mode due to the linear increase of its frequency with the external magnetic field. The exchange resonance mode is unambiguously identified by its THz frequency range at low temperature that gradually decreases to vanish at T_A, as well as due to the linear decrease of its frequency with the external magnetic field. We demonstrate that the damping parameters of these modes have different values that both highly depend on temperature and maximize near T_A. These results are interpreted in the framework of computational atomistic simulations and an analytical calculation based on the two-sublattice Landau-Lifshitz-Bloch equation. Moreover, we show that the damping of the ferromagnetic and exchange modes varies differently as a function of the external magnetic field. Their distinct behaviors are explained by considering the different features of the effective fields defining the precession frequency of the ferromagnetic and exchange modes.

II. SAMPLE CHARACTERIZATION AND EXPERIMENTAL METHODS

The insulating RE-Fe garnets belong to the centrosymmetric space group $Ia\bar{3}d$ (O_h^{10}), in which the magnetic atoms occupy three different crystallographic sites formed by the oxygen atoms (tetrahedral 24d, octahedral 16a, and dodecahedral 24c) [34,35]. The iron ions are distributed over the two nonequivalent tetrahedral and octahedral sublattices that are antiferromagnetically coupled by a strong negative superexchange interaction. The RE ions occupy the dodecahedral sublattice and their magnetic moments M_{RE} are antiferromagnetically coupled to the resultant iron magnetic moments M_{Fe} with a relatively weak superexchange interaction. Due to their strong superexchange interactions, the Fe^{3+} ions are usually treated as belonging to a single site, reducing the system to a two-sublattice ferrimagnet. The magnetization dynamics is usually represented by the following two coupled Landau-Lifshitz-Gilbert equations [36,37]:

$$\frac{dM_{Fe}}{dt} = -\gamma_{Fe}\left[\vec{M}_{Fe} \times \left(\vec{H}_{ext} + \vec{H}^a_{Fe} + \lambda_{exch}\vec{M}_{RE}\right)\right] + \frac{\alpha_{Fe}}{M_{Fe}}\left(M_{Fe} \times \frac{dM_{Fe}}{dt}\right),$$
$$\frac{dM_{RE}}{dt} = -\gamma_{RE}\left[\vec{M}_{RE} \times \left(\vec{H}_{ext} + \vec{H}^a_{RE} + \lambda_{exch}\vec{M}_{Fe}\right)\right] + \frac{\alpha_{RE}}{M_{RE}}\left(M_{RE} \times \frac{dM_{RE}}{dt}\right), \quad (1)$$

where H^a_i is the anisotropic field of the sublattice i (i = RE, Fe), H_{ext} is the external field, λ_{exch} is the molecular-field constant describing the RE-Fe interaction, and α_i is the damping parameter. Solving these coupled equations yields to two modes called the ferromagnetic mode and the exchange mode [36,37]. Among the different approximate solutions for the frequency of the ferromagnetic (f_{fmr}) and exchange (f_{exch}) modes [17,18,36–38], the ones which seem to provide the higher degree of accuracy give [37]

$$f_{fmr} = \gamma_{eff}\left(H_{ext} + \frac{M_{Fe}H^a_{Fe} - M_{RE}H^a_{RE}}{M_{Fe} - M_{RE}}\right), \quad (2)$$

$$f_{exch} = \lambda_{exch}\left(\gamma_{RE}M_{Fe} - \gamma_{Fe}M_{RE}\right) - \frac{\gamma_{Fe} + \gamma_{RE}}{2}H_{ext} + \frac{\gamma_{Fe}H^a_{Fe} - \gamma_{RE}H^a_{RE}}{2}, \quad (3)$$

where

$$\gamma_{eff}(T) = (M_{Fe} - M_{RE})/\left(\frac{M_{Fe}}{\gamma_{Fe}} - \frac{M_{RE}}{\gamma_{RE}}\right) \quad (4)$$

is the effective gyromagnetic ratio which can also be written as $\gamma_{eff} = M/A$ in terms of the net magnetic ($M = M_{Fe} - M_{RE}$) and net angular ($A = \frac{M_{Fe}}{\gamma_{Fe}} - \frac{M_{RE}}{\gamma_{RE}}$) momenta. These solutions include the effect of magnetic anisotropy. They also do not neglect the term with H_{ext} compared to the term λ_{exch} ($\gamma_{RE}M_{Fe} - \gamma_{Fe}M_{RE}$) to properly describe the dependences near T_M and T_A. The Equations (2) and (4) predict that f_{fmr} should increase linearly with increasing H_{ext}, go to zero at T_M, and diverge at T_A. Equation (3) predicts that f_{exch}, dominated by the first term $\lambda_{exch}(\gamma_{RE}M_{Fe} - \gamma_{Fe}M_{RE})$ due to the large value of λ_{exch}, has a weak linear decrease with H_{ext} as well as a softening near T_A. We note that the solution of the effective Gilbert damping for the ferromagnetic resonance mode is given by [39]

$$\alpha^{fmr}_{eff}(T) = \frac{\alpha_{Fe}\frac{M_{Fe}}{\gamma_{Fe}} + \alpha_{RE}\frac{M_{RE}}{\gamma_{RE}}}{\frac{M_{Fe}}{\gamma_{Fe}} - \frac{M_{RE}}{\gamma_{RE}}}. \quad (5)$$

Equation (5) shows a divergence of α^{fmr}_{eff} at T_A. A similar expression for $\alpha^{exch}_{eff}(T)$ seems still to be determined. We must mention that a recent study of the magnetization dynamics in ferrimagnets by both computer simulations and analytical calculations predicts no divergence of f_{fmr} and α^{fmr}_{eff} at T_A, but only a finite maximum [40]. This theoretical investigation also predicts that α^{exch}_{eff} has maximum at T_A and f_{fmr} does not go to zero at T_M, but has a finite value [40].

The experiments were performed on a 7-μm-thick ferrimagnetic $(GdTmPrBi)_3(FeGa)_5O_{12}$ single-crystalline film, grown by liquid-phase epitaxy (LPE) on a (111) gadolinium gallium garnet substrate. The static magneto-optical (MO) and magnetic properties of the film were characterized using a custom-designed magneto-optical Kerr spectrometer based on a 90° polarization modulation technique. Details on the experimental setup were described in Refs. [41,42]. Figure 1(a) shows the room-temperature Kerr rotation (Θ_K) and ellipticity (ε_K) spectra. Above the optical band gap ($E_g \approx 510$ nm), strong interference oscillations are observed for Θ_F and ε_F which both reach about 2.6° near 575 nm. Below the band gap,

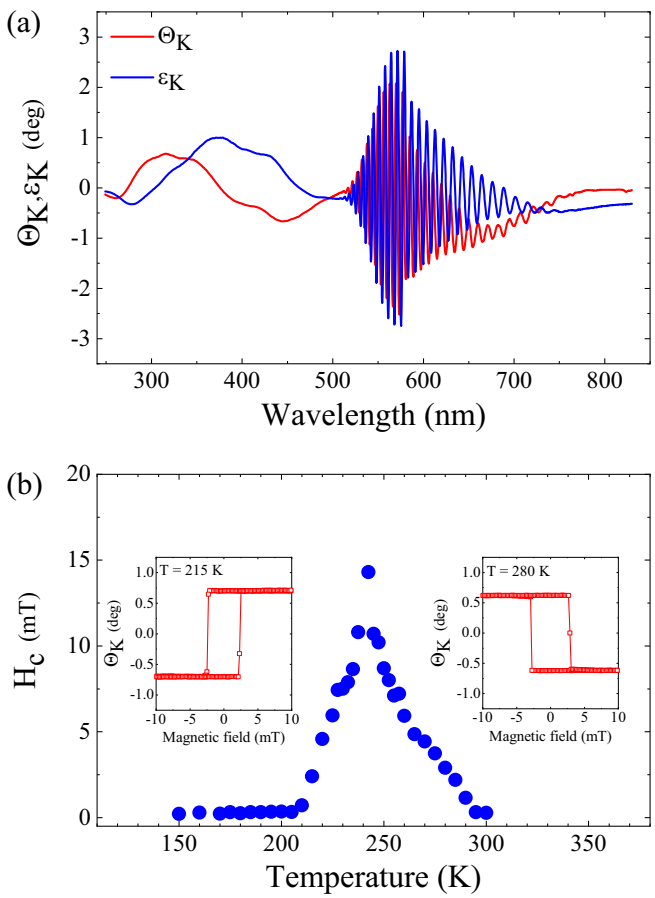

FIG. 1. Static magneto-optical and magnetic properties of the garnet film. (a) Magneto-optical polar Kerr rotation (Θ_K) and ellipticity (ε_K) spectra at 300 K. The strong interference oscillations in Θ_K and ε_K above 510 nm are due to the multiple reflexions in the film. (b) Temperature dependence of the coercive field H_c. The insets show polar Kerr hysteresis loops measured at a wavelength of 450 nm for H_{ext} applied normal to the film plane for a temperature below ($T = 215$ K) and above ($T = 280$ K) the compensation temperature T_M.

ε_K reaches a maximum value of 0.98° at 374 nm, whereas Θ_K shows two peaks with opposite sign and equal amplitude of 0.66°. The large Kerr signals and the interference above E_g are due to the multiple reflections in the film that occur in the Kerr responses. These spectral dependencies, in good agreement with previous studies of MO properties in Bi-substituted iron garnet [41,43], are well explained by the crystal energy levels of Fe^{3+} ions in the octahedral and tetrahedral symmetries and their strong hybridization with Bi-6*s* orbital [42,44–46]. The insets of Fig. 1(b) show two selected hysteresis loops measured at 215 and 280 K with an applied field perpendicular to the film plane. Their square shape reveals that the magnetic anisotropy is perpendicular to the film plane. We mention that all measured hysteresis loops below 300 K have almost the same amplitude, in agreement with the approach describing the MO spectra in terms of diamagnetic optical transitions [42,46,47]. Furthermore, we observe that the hysteresis loops change sign at the magnetic compensation temperature, $T_M \sim 245$ K, where a maximum of H_C also takes place [see Fig. 1(b)]. We note that in gadolinium iron garnets, T_M and T_A are nearly equal [48] or rather close to each other [49], which is also the case of our sample where the difference between T_M and T_A is less than 10 K.

The laser-induced spin dynamics were investigated by time-resolved magneto-optical Kerr (TR-MOKE) effect with the all-optical pump-probe configuration sketched in Fig. 2(a). We have employed a femtosecond laser pulse issued from an amplified Ti-sapphire laser system operating at a 5-kHz repetition rate and delivering 50-fs pulses at 800 nm to generate the pump and the probe beams. The pump beam was kept at the fundamental of the amplifier at 800 nm and excites the sample at an incidence angle of 7.5°, while the probe beam was frequency doubled to 400 nm using a beta-barium borate crystal and incident with a small angle of 1.5°. The pump beam was circularly polarized and focused onto the sample in a spot diameter of ~150 μm. The probe beam was linearly polarized and had a diameter of ~60 μm. The reflected probe beam allows measuring the differential changes of the magneto-optical polar Kerr rotation $\Delta\Theta_K(t)$ induced by the excitation pulse as a function of the time delay t between the pump and probe pulses using a polarization bridge and a lock-in detection scheme. The sample was mounted in a helium-cooled magneto-optical cryostat with temperature stability better than 0.2 K and equipped with 10-T superconducting magnet. H_{ext} was applied parallel to the film plane.

III. RESULTS AND DISCUSSION

Figures 2(b) and 2(c) display the TR-MOKE measurements of the magnetization dynamics induced by right (σ^+) and left (σ^-) circularly polarized light for $H_{ext} = 2$ T at $T = 290$ K [Fig. 2(b)] and $T = 190$ K [Fig. 2(c)]. For both temperatures, the signals show complex oscillations issued from two resonance modes, as revealed by the fast Fourier transform (FFT) [see the insets of Figs. 2(b) and 2(c)]. By reversing the helicity of the pump pulse, these oscillations change sign and keep the same amplitudes. In addition, the amplitude of the two modes linearly increases with increasing the pump energy density E_{pump} (not shown). These results indicate that the main mechanism behind the excitation is the inverse Faraday effect, where a circularly polarized light generates a magnetic field in the direction of the propagating pump beam [41,50,51]. This field has opposite signs for σ^+ and σ^- which result in a π-phase shift for the spin precession as seen in Figs. 2(b) and 2(c). To study in detail the properties of these modes, TR-MOKE signals are fitted using the sum of two exponentially damped oscillators:

$$\Delta\Theta_K(t) = \sum_{i=1}^{2} A_i e^{-t/\tau_i} \sin(2\pi f_i t - \phi_i) + B e^{-Ct}, \quad (6)$$

where A_i, f_i, ϕ_i, τ_i are, respectively, the amplitude, frequency, initial phase, and decay time characterizing the precession of the mode i ($i = 1, 2$). The term Be^{-Ct} represents a MO background signal added for best fit. This term was previously reported in many magnetic insulators [50,52–54] and it likely has an electronic origin [53]. The fits with Eq. (6) are plotted in Figs. 2(b) and 2(c) with solid lines showing a good agreement with the experimental data. It allows

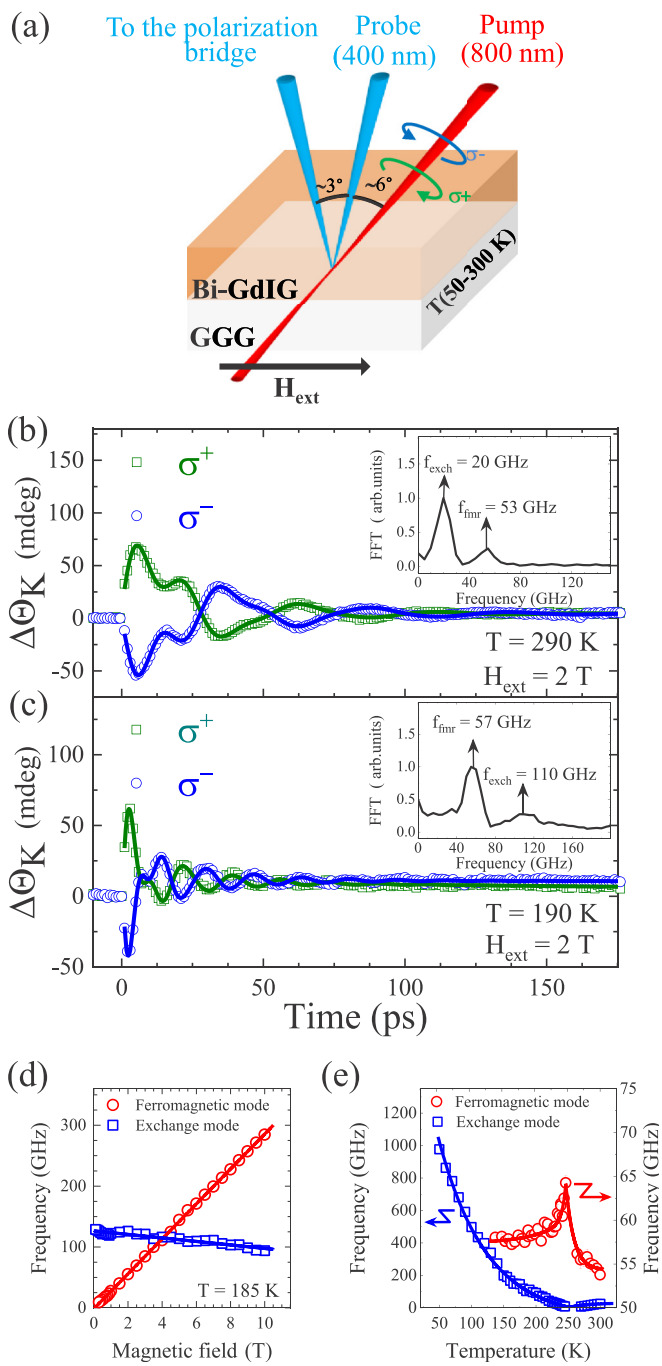

FIG. 2. Laser-induced spin dynamic in the garnet film. (a) Sketch of the time-resolved magneto-optical Kerr configuration. (b), (c) $\Delta\Theta_K$ induced by $E_{pump} = 38\,\mathrm{mJ\,cm^{-2}}$ for $H_{ext} = 2$ T and temperatures of (b) $T = 290$ K and (c) $T = 190$ K. The solid lines are the fits using Eq. (6). (d) Magnetic field dependence of f_{fmr} and f_{exch} for $T = 185$ K. The solid lines are the fits using Eqs. (2) and (3). (e) Temperature dependence of f_{fmr} and f_{exch}. The solid lines are guides to the eye. The insets show the FFT spectra.

extracting the frequencies of $f_1 = f_{fmr} = 53$ GHz (57.8 GHz) and $f_2 = f_{exch} = 20$ GHz (110.3 GHz) at 290 K (190 K). These frequencies correspond precisely to those derived by the FFT analysis. The adjustments also allow extracting

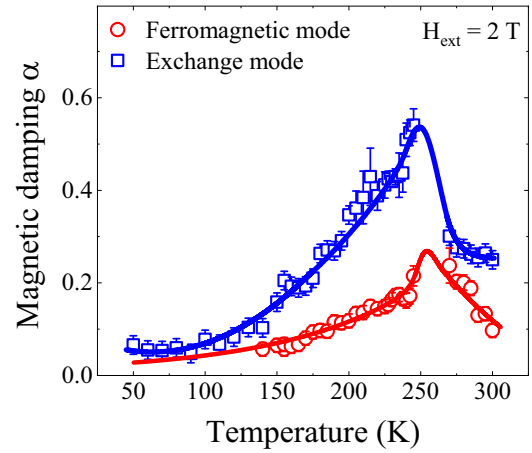

FIG. 3. Magnetic damping of the ferromagnetic (α_{fmr}) and exchange (α_{exch}) resonance modes as a function of temperature for $H_{ext} = 2$ T and $E_{pump} = 32\,\mathrm{mJ\,cm^{-2}}$. The solid lines are guides to the eye.

the effective damping of each resonance mode, defined as $\alpha_i = {}^1/_{f_i\tau_i}$.

To determine the physical origin of the two modes, we investigated the dependence of their frequency as a function of the external field [Fig. 2(d)] and temperature [Fig. 2(e)]. The mode with the frequency that increases linearly with increasing H_{ext} matches the behavior of the ferromagnetic mode [see Eq. (2)], while the one with the frequency that slightly decreases with increasing H_{ext} is consistent with the behavior of the exchange mode [see Eq. (3)]. These origins are confirmed by their temperature dependences where f_{exch} is in the THz range at low temperature and progressively decreases until vanishing near T_A, whereas f_{fmr} shows a clear maximum near T_A [Fig. 2(e)]. Considering the near proximity of T_M and T_A in gadolinium iron garnets [48,49], the temperature dependence of f_{fmr} is consistent with the one measured in the GdFeCo [17] and CoGd [18] metallic alloys. It is also in good agreement with the results obtained from recent atomistic simulations and a theory based on the two-sublattice Landau-Lifshitz-Bloch equations [40].

Figure 3 shows the temperature dependence of the ferromagnetic (α_{fmr}) and exchange (α_{exch}) damping. Interestingly, both show a pronounced maximum at T_A, where their ratio is rather large, with an exchange mode being ~2.7× more damped than the ferromagnetic one. These behaviors, observed here in a ferrimagnetic garnet, have been recently predicted theoretically [40]. Note that the observed maximum of α_{fmr} and f_{fmr} at a temperature not very far below room temperature suggest that this system might be interesting for ringing-free precessional switching where high damping is required.

To study in more detail the damping parameters, we investigate their dependencies on H_{ext} up to 10 T at a temperature below [$T = 150$ K, Fig. 4(a)] and above [$T = 300$ K, Fig. 4(b)] T_A. α_{fmr} shows a very pronounced exponential-like decrease by 92% at 150 K and 95% at 300 K. For $H_{ext} = 10$ T it reaches small values of 0.025 and 0.036 at 150 and 300 K, respectively. Similar field dependences of

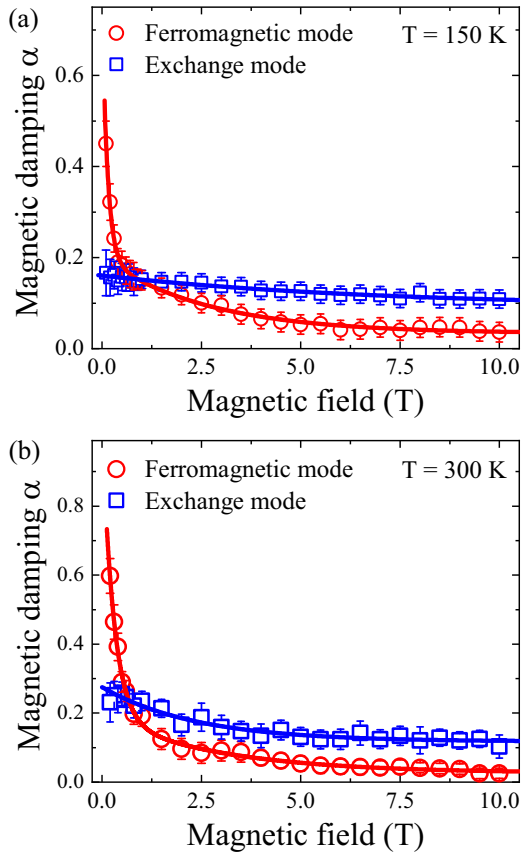

FIG. 4. Magnetic damping of the ferromagnetic (α_{fmr}) and exchange (α_{exch}) resonance modes as a function of H_{ext} at (a) $T = 150$ K and (b) $T = 300$ K for a pump energy density $E_{pump} = 32$ mJ cm^{-2}. The solid lines are guides to the eye.

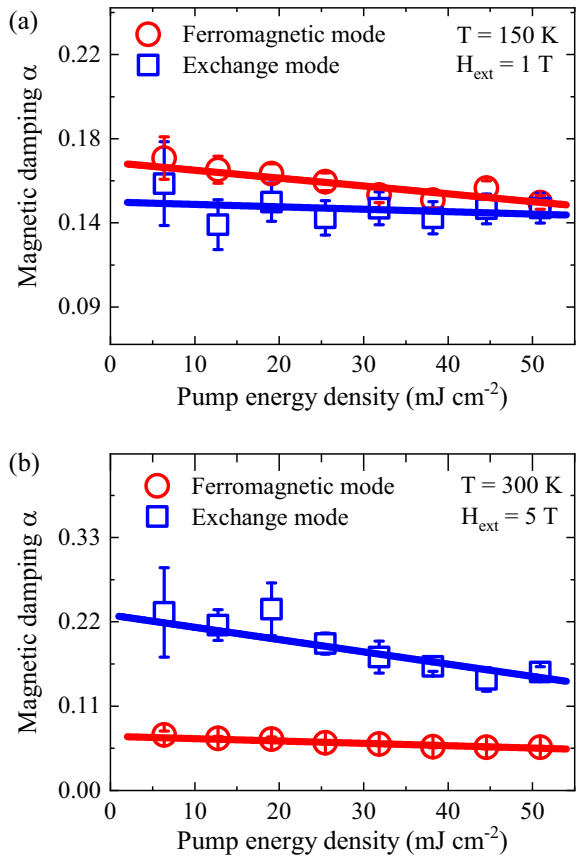

FIG. 5. Magnetic damping of the ferromagnetic (α_{fmr}) and exchange (α_{exch}) resonance modes measured as a function of the pump energy density E_{pump} at (a) 150 K and (b) 300 K. The damping at 150 K is obtained for $H_{ext} = 1$ T, whereas the damping at 300 K is obtained for $H_{ext} = 5$ T. The solid lines are guides to the eye.

α_{fmr} were previously observed in different magnetic media [55–58]. The increase of α_{fmr} at low H_{ext} can be attributed to a weak inhomogeneity in the magnetic anisotropy field, which defines the precession frequency of the ferromagnetic mode [57]. This magnetic inhomogeneity induces a broadening of the ferromagnetic precession frequency, which increases the magnetic losses via magnon-magnon scattering. When the applied field H_{ext} becomes larger and larger, the frequency of the ferromagnetic precession becomes more and more defined by this field, which is almost homogeneous across the sample. This ensures better and better coherence of the magnetization precession, limiting the magnetic losses, and thus reducing the magnetic damping to its intrinsic value. Indeed, the obtained values of α_{fmr} at high H_{ext} are in good agreement with the ones reported in the literature for GdIG [59], Bi-substituted GdIG [60], and (Yb,Bi)-substituted GdIG [61].

The field dependence of α_{exch} shows also a decrease, which is relatively small compared to the one measured for α_{fmr} [see Figs. 4(a) and 4(b)]. On the other hand, the decrease of α_{exch} is more pronounced at 300 K than at 150 K. This behavior can be qualitatively explained considering features of the precession frequency of the exchange mode. For temperatures far from T_A, such as150 K, f_{exch} is mainly defined by the Gd-Fe superexchange coupling parameter λ_{exch} [see Eq. (3)], which is determined by the local Fe-O-Gd distances. Considering the well-known high stability of the garnet structure [35,62], together with the very good crystallinity of garnets grown by LPE [63], λ_{exch} should be almost homogeneous over the film. This guarantees a coherent exchange precession independently on H_{ext}, and therefore α_{exch} will slightly depend on the external magnetic field. For temperatures near T_A, such as 300 K, the term $\lambda_{exch}(\gamma_2 M_1 - \gamma_1 M_2)$ becomes small and comparable to the last terms in Eq. (3), which involves the anisotropy field. Due to a small inhomogeneity of the anisotropy field, a bordering of the exchange precession frequency occurs at low H_{ext}, which increases α_{exch} due to the magnon-magnon scattering. The increase of H_{ext} results in a better coherence of f_{exch}, and therefore α_{exch} converges toward its intrinsic value with a more significant decrease compared to 150 K.

To further investigate the damping of both modes, we studied their dependence on E_{pump} at 150 and 300 K. The dependences at 150 K are obtained for $H_{ext} = 1$ T [Fig. 5(a)], whereas the ones at 300 K are obtained for $H_{ext} = 5$ T [Fig. 5(b)]. The results show a linear decrease of α_{fmr} with increasing E_{pump} at both 150 and 300 K. This dependence is different compared to the ones usually measured in metallic magnets, where α_{fmr} increases with increasing E_{pump} [64,65]. The behavior in metallic magnets can be qualitatively linked

to an increase of the sample temperature toward the Curie temperature, where α_{fmr} is expected to have a larger value [40,66]. In Bi-substituted iron garnets, the absorption of the 800-nm pump pulses by the phonon-assisted electronic *d-d* transitions can induce a small increase of the sample temperature [20,26,67]. This temperature rise can explain the decrease of α_{fmr} and α_{exch} with E_{pump} at 300 K as the sample temperature will be rather far from T_{A} where the damping tends to have smaller values. Within this picture, for the measurements at 150 K, a small temperature rise with E_{pump} should induce an increase of α_{fmr} and α_{exch} as the sample temperature will approach T_{A}; however, the opposite behavior is observed. This suggests that additional mechanisms are involved in the dependence of the damping on the pump energy density. A possible scenario to explain this dependence apart from the sample temperature variation can be described as follows: For high E_{pump}, the magnetization is more homogeneously excited around the probed area, leading to a better coherence of the spin precession and therefore a lower magnetic damping than the one measured at low E_{pump}. However, a further inquiry is necessary to understand in more detail the effect of E_{pump} on the damping of magnetic insulators.

IV. CONCLUSIONS

We have studied the laser-induced ferromagnetic and exchange resonance modes in the bismuth-substituted gadolinium iron garnet over a wide range of magnetic fields (0–10 T) and temperatures (50–300 K) including the magnetization and angular compensation points. These two magnetic modes were excited via the inverse Faraday effect and unambiguously identified by their distinct frequency dependence on temperature and external magnetic field. We demonstrate that the damping of these modes has different values that both highly depend on temperature and maximizes near the angular compensation point. These properties confirm recent predictions of atomistic simulations and an analytical calculation based on the two-sublattice Landau-Lifshitz-Bloch equation. We also demonstrate that the damping of the two modes have different behaviors as a function of the external magnetic field. We explain this phenomenon considering the different features of the effective fields defining the precession frequency of the ferromagnetic and exchange modes. Our results provide a detailed characterization of both ferromagnetic and exchange resonance modes, which predict a high-speed precessional magnetization reversal near the angular compensation point, as the ferromagnetic mode combines a large damping with high precession frequency.

ACKNOWLEDGMENT

M.D. acknowledges the Alexander von Humboldt Foundation for financial support.

[1] T. L. Gilbert, A phenomenological theory of damping in ferromagnetic materials, IEEE Trans. Magn. **40**, 3443 (2004).
[2] F. Bloch, Nuclear induction, Phys. Rev. **70**, 460 (1946).
[3] A. Mougin, M. Cormier, J. P. Adam, P. J. Metaxas, and J. Ferré, Domain wall mobility, stability and Walker breakdown in magnetic nanowires, Europhys. Lett. (EPL) **78**, 57007 (2007).
[4] T. Weindler, H. G. Bauer, R. Islinger, B. Boehm, J. Y. Chauleau, and C. H. Back, Magnetic Damping: Domain Wall Dynamics versus Local Ferromagnetic Resonance, Phys. Rev. Lett. **113**, 237204 (2014).
[5] H. Y. Yuan, Z. Yuan, K. Xia, and X. R. Wang, Influence of nonlocal damping on the field-driven domain wall motion, Phys. Rev. B **94**, 064415 (2016).
[6] H. W. Schumacher, C. Chappert, P. Crozat, R. C. Sousa, P. P. Freitas, J. Miltat, J. Fassbender, and B. Hillebrands, Phase Coherent Precessional Magnetization Reversal in Microscopic Spin Valve Elements, Phys. Rev. Lett. **90**, 017201 (2003).
[7] C. H. Back, D. Weller, J. Heidmann, D. Mauri, D. Guarisco, E. L. Garwin, and H. C. Siegmann, Magnetization Reversal in Ultrashort Magnetic Field Pulses, Phys. Rev. Lett. **81**, 3251 (1998).
[8] A. V. Chumak, V. I. Vasyuchka, A. A. Serga, and B. Hillebrands, Magnon spintronics, Nat. Phys. **11**, 453 (2015).
[9] J. Han, P. Zhang, J. T. Hou, S. A. Siddiqui, and L. Liu, Mutual control of coherent spin waves and magnetic domain walls in a magnonic device, Science **366**, 1121 (2019).
[10] D. Houssameddine, U. Ebels, B. Delaët, B. Rodmacq, I. Firastrau, F. Ponthenier, M. Brunet, C. Thirion, J. P. Michel, L. Prejbeanu-Buda *et al.*, Spin-torque oscillator using a perpendicular polarizer and a planar free layer, Nat. Mater. **6**, 447 (2007).
[11] S. I. Kiselev, J. C. Sankey, I. N. Krivorotov, N. C. Emley, R. J. Schoelkopf, R. A. Buhrman, and D. C. Ralph, Microwave oscillations of a nanomagnet driven by a spin-polarized current, Nature (London) **425**, 380 (2003).
[12] Y. Li, F. Zeng, S. S. L. Zhang, H. Shin, H. Saglam, V. Karakas, O. Ozatay, J. E. Pearson, O. G. Heinonen, Y. Wu *et al.*, Giant Anisotropy of Gilbert Damping in Epitaxial CoFe Films, Phys. Rev. Lett. **122**, 117203 (2019).
[13] C. K. Mewes and T. Mewes, Relaxation in magnetic materials for spintronics, in *Handbook of Nanomagnetism: Applications and Tools* (Pan Stanford, Boca Raton, FL, 2015), pp. 71–95.
[14] O. Boulle, V. Cros, J. Grollier, L. G. Pereira, C. Deranlot, F. Petroff, G. Faini, J. Barnaś, and A. Fert, Shaped angular dependence of the spin-transfer torque and microwave generation without magnetic field, Nat. Phys. **3**, 492 (2007).
[15] S. Neusser and D. Grundler, Magnonics: Spin waves on the nanoscale, Adv. Mater. **21**, 2927 (2009).
[16] A. V. Chumak, A. A. Serga, and B. Hillebrands, Magnon transistor for all-magnon data processing, Nat. Commun. **5**, 4700 (2014).
[17] C. D. Stanciu, A. V. Kimel, F. Hansteen, A. Tsukamoto, A. Itoh, A. Kirilyuk, and T. Rasing, Ultrafast spin dynamics across compensation points in ferrimagnetic GdFeCo: The role of angular momentum compensation, Phys. Rev. B **73**, 220402(R) (2006).
[18] M. Binder, A. Weber, O. Mosendz, G. Woltersdorf, M. Izquierdo, I. Neudecker, J. R. Dahn, T. D. Hatchard, J. U. Thiele, C. H. Back *et al.*, Magnetization dynamics of the ferrimagnet CoGd near the compensation of magnetization and angular momentum, Phys. Rev. B **74**, 134404 (2006).

[19] M. Deb, E. Popova, M. Hehn, N. Keller, S. Petit-Watelot, M. Bargheer, S. Mangin, and G. Malinowski, Damping of Standing Spin Waves in Bismuth-Substituted Yttrium Iron Garnet as Seen Via the Time-Resolved Magneto-Optical Kerr Effect, Phys. Rev. Appl. **12**, 044006 (2019).

[20] M. Deb, E. Popova, M. Hehn, N. Keller, S. Petit-Watelot, M. Bargheer, S. Mangin, and G. Malinowski, Femtosecond Laser-Excitation-Driven High Frequency Standing Spin Waves in Nanoscale Dielectric Thin Films of Iron Garnets, Phys. Rev. Lett. **123**, 027202 (2019).

[21] G. Malinowski, K. C. Kuiper, R. Lavrijsen, H. J. M. Swagten, and B. Koopmans, Magnetization dynamics and Gilbert damping in ultrathin $Co_{48}Fe_{32}B_{20}$ films with out-of-plane anisotropy, Appl. Phys. Lett. **94**, 102501 (2009).

[22] T. Schneider, A. A. Serga, B. Leven, B. Hillebrands, R. L. Stamps, and M. P. Kostylev, Realization of spin-wave logic gates, Appl. Phys. Lett. **92**, 022505 (2008).

[23] A. A. Serga, A. V. Chumak, and B. Hillebrands, YIG magnonics, J. Phys. D: Appl. Phys. **43**, 264002 (2010).

[24] A. Hassdenteufel, B. Hebler, C. Schubert, A. Liebig, M. Teich, M. Helm, M. Aeschlimann, M. Albrecht, and R. Bratschitsch, Thermally assisted all-optical helicity dependent magnetic switching in amorphous $Fe_{100-x}Tb_x$ alloy films, Adv. Mater. **25**, 3122 (2013).

[25] Y. Xu, M. Deb, G. Malinowski, M. Hehn, W. Zhao, and S. Mangin, Ultrafast magnetization manipulation using single femtosecond light and hot-electron pulses, Adv. Mater. **29**, 1703474 (2017).

[26] M. Deb, P. Molho, B. Barbara, and J.-Y. Bigot, Controlling laser-induced magnetization reversal dynamics in a rare-earth iron garnet across the magnetization compensation point, Phys. Rev. B **97**, 134419 (2018).

[27] C. D. Stanciu, A. Tsukamoto, A. V. Kimel, F. Hansteen, A. Kirilyuk, A. Itoh, and T. Rasing, Subpicosecond Magnetization Reversal across Ferrimagnetic Compensation Points, Phys. Rev. Lett. **99**, 217204 (2007).

[28] K.-J. Kim, S. K. Kim, Y. Hirata, S.-H. Oh, T. Tono, D.-H. Kim, T. Okuno, W. S. Ham, S. Kim, G. Go *et al.*, Fast domain wall motion in the vicinity of the angular momentum compensation temperature of ferrimagnets, Nat. Mater. **16**, 1187 (2017).

[29] S. A. Siddiqui, J. Han, J. T. Finley, C. A. Ross, and L. Liu, Current-Induced Domain Wall Motion in a Compensated Ferrimagnet, Phys. Rev. Lett. **121**, 057701 (2018).

[30] R. Mishra, J. Yu, X. Qiu, M. Motapothula, T. Venkatesan, and H. Yang, Anomalous Current-Induced Spin Torques in Ferrimagnets near Compensation, Phys. Rev. Lett. **118**, 167201 (2017).

[31] R. Bläsing, T. Ma, S.-H. Yang, C. Garg, F. K. Dejene, A. T. N'Diaye, G. Chen, K. Liu, and S. S. P. Parkin, Exchange coupling torque in ferrimagnetic Co/Gd bilayer maximized near angular momentum compensation temperature, Nat. Commun. **9**, 4984 (2018).

[32] T. Okuno, D.-H. Kim, S.-H. Oh, S. K. Kim, Y. Hirata, T. Nishimura, W. S. Ham, Y. Futakawa, H. Yoshikawa, A. Tsukamoto *et al.*, Spin-transfer torques for domain wall motion in antiferromagnetically coupled ferrimagnets, Nat. Electron. **2**, 389 (2019).

[33] D.-H. Kim, T. Okuno, S. K. Kim, S.-H. Oh, T. Nishimura, Y. Hirata, Y. Futakawa, H. Yoshikawa, A. Tsukamoto, Y. Tserkovnyak *et al.*, Low Magnetic Damping of Ferrimagnetic GdFeCo Alloys, Phys. Rev. Lett. **122**, 127203 (2019).

[34] F. Bertaut and F. Forrat, Structure des ferrites ferrimagnetiques des terres rares, C. R. Acad. Sci., Paris **242**, 382 (1956).

[35] G. D. Winkler, *Magnetic Garnets* (Vieweg, Braunschweig, 1981).

[36] R. K. Wangsness, Sublattice effects in magnetic resonance, Phys. Rev. **91**, 1085 (1953).

[37] S. Geschwind and L. R. Walker, Exchange resonances in gadolinium iron garnet near the magnetic compensation temperature, J. Appl. Phys. **30**, S163 (1959).

[38] J. Kaplan and C. Kittel, Exchange frequency electron spin resonance in ferrites, J. Chem. Phys. **21**, 760 (1953).

[39] A. G. Gurevich and G. A. Melkov, *Magnetization Oscillations and Waves* (CRC Press, London, 1996).

[40] F. Schlickeiser, U. Atxitia, S. Wienholdt, D. Hinzke, O. Chubykalo-Fesenko, and U. Nowak, Temperature dependence of the frequencies and effective damping parameters of ferrimagnetic resonance, Phys. Rev. B **86**, 214416 (2012).

[41] M. Deb, M. Vomir, J.-L. Rehspringer, and J.-Y. Bigot, Ultrafast optical control of magnetization dynamics in polycrystalline bismuth doped iron garnet thin films, Appl. Phys. Lett. **107**, 252404 (2015).

[42] M. Deb, E. Popova, and N. Keller, Different magneto-optical response of magnetic sublattices as a function of temperature in ferrimagnetic bismuth iron garnet films, Phys. Rev. B **100**, 224410 (2019).

[43] F. Hansteen, L. E. Helseth, T. H. Johansen, O. Hunderi, A. Kirilyuk, and T. Rasing, Optical and magnetooptical properties of bismuth and gallium substituted iron garnet films, Thin. Solid. Films **455**, 429 (2004).

[44] G. A. Allen and G. F. Dionne, Application of permittivity tensor for accurate interpretation of magneto-optical spectra, J. Appl. Phys. **73**, 6130 (1993).

[45] G. F. Dionne and G. A. Allen, Molecular-orbital analysis of magneto-optical Bi-O-Fe hybrid excited states, J. Appl. Phys. **75**, 6372 (1994).

[46] M. Deb, E. Popova, A. Fouchet, and N. Keller, Magneto-optical Faraday spectroscopy of completely bismuth-substituted Bi_3Fe_5O garnet thin films, J. Phys. D: Appl. Phys. **45**, 455001 (2012).

[47] G. F. Dionne and G. A. Allen, Spectral origins of giant Faraday rotation and ellipticity in Bi-substituted magnetic garnets, J. Appl. Phys. **73**, 6127 (1993).

[48] B. A. Calhoun, J. Overmeyer, and W. V. Smith, Ferrimagnetic resonance in gadolinium iron garnet, Phys. Rev. **107**, 993 (1957).

[49] B. A. Calhoun, W. V. Smith, and J. Overmeyer, Ferrimagnetic resonance in gadolinium iron garnet, J. Appl. Phys. **29**, 427 (1958).

[50] A. V. Kimel, A. Kirilyuk, P. A. Usachev, R. V. Pisarev, A. M. Balbashov, and T. Rasing, Ultrafast non-thermal control of magnetization by instantaneous photomagnetic pulses, Nature (London) **435**, 655 (2005).

[51] F. Hansteen, A. Kimel, A. Kirilyuk, and T. Rasing, Nonthermal ultrafast optical control of the magnetization in garnet films, Phys. Rev. B **73**, 014421 (2006).

[52] A. M. Kalashnikova, A. V. Kimel, R. V. Pisarev, V. N. Gridnev, A. Kirilyuk, and T. Rasing, Impulsive Generation of Coherent

Magnons by Linearly Polarized Light in the Easy-Plane Antiferromagnet $FeBO_3$, Phys. Rev. Lett. **99**, 167205 (2007).

[53] B. Koene, M. Deb, E. Popova, N. Keller, T. Rasing, and A. Kirilyuk, Excitation of magnetic precession in bismuth iron garnet via a polarization-independent impulsive photomagnetic effect, Phys. Rev. B **91**, 184415 (2015).

[54] B. Koene, M. Deb, E. Popova, N. Keller, T. Rasing, and A. Kirilyuk, Spectrally resolved optical probing of laser induced magnetization dynamics in bismuth iron garnet, J. Phys.: Condens. Matter **28**, 276002 (2016).

[55] P. Nčmec, V. Novák, N. Tesařová, E. Rozkotová, H. Reichlová, D. Butkovičová, F. Trojánek, K. Olejník, P. Malý, R. P. Campion *et al.*, The essential role of carefully optimized synthesis for elucidating intrinsic material properties of (Ga,Mn)As, Nat. Commun. **4**, 1422 (2013).

[56] R. R. Subkhangulov, H. Munekata, T. Rasing, and A. V. Kimel, Laser-induced spin dynamics in ferromagnetic (In,Mn)As at magnetic fields up to 7 T, Phys. Rev. B **89**, 060402(R) (2014).

[57] J. Walowski, M. D. Kaufmann, B. Lenk, C. Hamann, J. McCord, and M. Münzenberg, Intrinsic and non-local Gilbert damping in polycrystalline nickel studied by Ti : sapphire laser fs spectroscopy, J. Phys. D: Appl. Phys. **41**, 164016 (2008).

[58] G. Counil, J.-V. Kim, T. Devolder, C. Chappert, K. Shigeto, and Y. Otani, Spin wave contributions to the high-frequency magnetic response of thin films obtained with inductive methods, J. Appl. Phys. **95**, 5646 (2004).

[59] H. Maier-Flaig, S. Geprägs, Z. Qiu, E. Saitoh, R. Gross, M. Weiler, H. Huebl, and S. Goennenwein, Perpendicular magnetic anisotropy in insulating ferrimagnetic gadolinium iron garnet thin films, arXiv:1706.08488.

[60] V. J. Fratello, S. E. G. Slusky, C. D. Brandle, and M. P. Norelli, Growth-induced anisotropy in bismuth: Rare-earth iron garnets, J. Appl. Phys. **60**, 2488 (1986).

[61] T. Satoh, Y. Terui, R. Moriya, B. A. Ivanov, K. Ando, E. Saitoh, T. Shimura, and K. Kuroda, Directional control of spin-wave emission by spatially shaped light, Nat. Photonics **6**, 662 (2012).

[62] G. F. Dionne, *Magnetic Oxides* (Springer, New York, 2009).

[63] P. Capper and M. Mauk, *Liquid Phase Epitaxy of Electronic, Optical and Optoelectronic Materials* (John Wiley & Sons, London, 2007), Vol. 21.

[64] B. Liu, X. Ruan, Z. Wu, H. Tu, J. Du, J. Wu, X. Lu, L. He, R. Zhang, and Y. Xu, Transient enhancement of magnetization damping in CoFeB film via pulsed laser excitation, Appl. Phys. Lett. **109**, 042401 (2016).

[65] S. Mondal and A. Barman, Laser Controlled Spin Dynamics of Ferromagnetic Thin Film from Femtosecond to Nanosecond Timescale, Phys. Rev. Appl. **10**, 054037 (2018).

[66] N. A. Natekar, W.-H. Hsu, and R. H. Victora, Calculated dependence of FePt damping on external field magnitude and direction, AIP Adv. **7**, 056004 (2017).

[67] C. S. Davies, K. H. Prabhakara, M. D. Davydova, K. A. Zvezdin, T. B. Shapaeva, S. Wang, A. K. Zvezdin, A. Kirilyuk, T. Rasing, and A. V. Kimel, Anomalously Damped Heat-Assisted Route for Precessional Magnetization Reversal in an Iron Garnet, Phys. Rev. Lett. **122**, 027202 (2019).